Soft Matter

PAPER

View Article Online
View Journal | View Issue

Cite this: *Soft Matter*, 2025, **21**, 6689

Errors matter when measuring Poisson's ratio of nearly incompressible elastomers

Robert D. Nedoluha, Majed N. Saadawi and Christopher W. Barney *

Poisson's ratio (ν) is a materials property that quantifies the compressibility of a material. Measurements of this property become important for soft elastomers which display nearly incompressible behavior ($\nu > 0.495$). Small differences in this property can lead to large differences in the stresses that develop during hydrostatic loadings such as those observed in gaskets, o-rings, and thin films. While there are multiple methods that can be used to quantify ν, many methods were developed for compressible materials which require less precision than nearly incompressible materials. Here an experimental survey of three methods of characterizing ν of a nearly incompressible elastomer is performed. These methods include direct measurement *via* digital image correlation, indirect measurement from the bulk modulus and Young's modulus, and a recently proposed method of indirect measurement from the shear modulus and Young's modulus. Particular care is paid towards understanding how experimental errors impact both the precision and accuracy of each method. It is found that indirectly measuring ν from the bulk modulus and Young's modulus is the most appropriate method for distinguishing nearly incompressible behavior from the incompressible limit ($\nu = 0.5$).

Received 22nd May 2025,
Accepted 3rd August 2025

DOI: 10.1039/d5sm00535c

rsc.li/soft-matter-journal

Soft solids are a class of materials where their bulk modulus is orders of magnitudes larger than either their shear or Young's moduli.[1] This difference results in nearly incompressible behavior ($\nu > 0.495$) as the energy penalty for changing shape is much lower than that for changing volume. Assuming a soft solid is incompressible ($\nu = 0.5$) is often reasonable; however, there are loadings where this assumption breaks down. Particularly in structures involving hydrostatic loadings such as those observed in gaskets, o-rings, and thin coatings.[2–4] Small changes in material compressibility, as quantified through differences in Poisson's ratio, can lead to significant differences in the stresses that develop in such geometries.[4] These small changes demand the precise characterization of Poisson's ratio to accurately model the stresses that develop during hydrostatic loadings.

While measuring the Poisson's ratio of nearly incompressible materials is important, it is also challenging. One challenge is that as a material approaches the incompressible limit, an increase in the precision of the measurement technique is needed to meaningfully characterize this property. In the infinitesimal strain limit, Poisson's ratio can be defined as the negative of the ratio between the transverse and axial strains during uniaxial extension.[5] Using this definition and assuming stretching is applied in the 1 direction gives,

$$\varepsilon_{vol} = \varepsilon_1 + \varepsilon_2 + \varepsilon_3 = \varepsilon_1(1 - 2\nu), \quad (1)$$

where ε_{vol} is the volumetric strain, ε_1 is the applied strain, and ν is Poisson's ratio. In the incompressible limit, $\varepsilon_{vol} = 0$ and the volumetric strain is independent of the applied strain. Eqn (1) shows that the incompressible condition is satisfied when $\nu = 0.5$. While soft solids are often assumed to be incompressible,[6] setting $\nu = 0.5$ implies an infinite energy penalty for changing volume. This can be seen in the relationship between the bulk modulus K and Young's modulus E,[7]

$$K = \frac{E}{3(1 - 2\nu)}, \quad (2)$$

where K diverges as $\nu \to 0.5$. For crosslinked rubbery networks, K is often $\sim$1 GPa while E is $\sim$1 MPa.[8] Using these values gives a value of Poisson's ratio of $0.49998\bar{3}$ which is only distinguishable from the 0.5 limit with a measurement error of 0.0001 or less. For compressible materials ($\nu < 0.495$), resolving ν to the fourth decimal point is unnecessary and measurements with lower precision can be performed. This implies that nearly incompressible materials need to be matched with measurement techniques that provide sufficient resolution to characterize Poisson's ratio as it approaches the limiting value of 0.5.

Methods developed to characterize ν largely fall into two categories. Direct methods include techniques where ν is directly quantified from the deformation of a material during loading. This category includes techniques such as digital image correlation (DIC),[9–13] strain gauge analysis,[14–16] and

School of Polymer Science and Polymer Engineering, 250 S Forge St, Akron, OH 44325, USA. E-mail: barneyc@uakron.edu; Tel: +1(330)972-4297

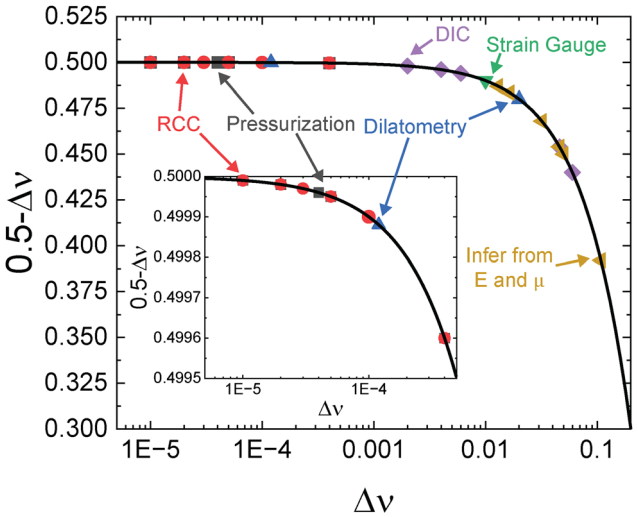

Fig. 1 Plot showing $0.5 - \Delta\nu$ *vs.* $\Delta\nu$ from literature data for RCC,[7,8,24,25] pressurization,[23–25] DIC,[9,11,12] strain gauge analysis,[30] dilatometry,[17,30] and inferred from E and μ.[28,29]

dilatometry.[17,18] Indirect methods include techniques that infer the value of ν from the measurement of at least two elastic moduli. This category includes techniques such as pressurization[19–22] to measure K combined with separate measurements of either E or the shear modulus μ,[23–25] radially confined compression (RCC)[2,8,24–27] to measure K combined with a separate measurement of E, and an emerging trend[28,29] of combining measurements of E and μ to infer ν. The methods used in this work measure low strain values of Poisson's ratio and have varied sensitivity to experimental errors.

Reported values of the error for each of these methods is displayed in Fig. 1 where $0.5 - \Delta\nu$ is plotted against the measurement error $\Delta\nu$. This compiled literature data is summarized in the SI. Note that these literature values are gathered on materials with varied chemical compositions and should thus have different values of ν. The black line on which this data falls represents the maximum value of ν that is distinguishable from the incompressible limit of 0.5 as a function of measurement error. As is apparent in Fig. 1, RCC and pressurization offer the highest levels of resolution. The next most precise method is dilatometry which occupies a large range of 2–4 decimal points of resolution. DIC follows this method with the ability to resolve 2–3 decimal points of ν. Strain gauge analysis appears to measure ν out to 2 decimal points. Finally, the emerging trend of inferring ν from measurements of E and μ can resolve 1–2 decimal points. Notably, the reported values for inferring ν from E and μ have all been generated from measurements in different setups (*e.g.* combining data from tensile tests and rheology[28] or tensile tests and lap shear tests[29]) and have not been attempted in a single setup. Based on this, we aim to infer ν from measurements of E and μ on a single sample and compare this to the resolution of other methods for quantifying ν of nearly incompressible elastomers.

Achieving this aim will require selecting several different methods to characterize ν. The first method presented is DIC during uniaxial extension as it is a highly accessible method that is similar to strain gauge analysis. The second method presented is to infer ν from measurements of K and E. In this work, RCC is used to measure K as previous works[24,25] have concluded that pressurization and RCC offer similar resolutions while RCC requires less specialized instrumentation. Dilatometry will not be performed in this work as it requires specialized instrumentation and spans a range of precision already covered by RCC and DIC. The final measurement method will exploit a combined tension and torsion tester to measure E in tension and μ in torsion on a single sample. All three methods are performed on the same commercially available rubbery crosslinked silicone elastomer that neither flows at long time scales nor exchanges mass with the surrounding environment. Such materials are known to be nearly incompressible ($\nu > 0.495$)[8] and are a reasonable model for this analysis. A comparison of all three of these methods including a discussion of the observed error associated with each technique is presented at the end. Note that these methods characterize the low strain elastic behavior of materials. These findings have strong implications for characterizing the mechanical response of gaskets, o-rings, and thin coatings.[2,26,31]

1 Materials and Instrumentation

1.1 Materials

Polydimethylsiloxane (PDMS) samples were formed using a commercially available Sylgard 184 kit.[32,33] Samples were formed at a weight ratio of 10 : 1 prepolymer : curing agent. Samples were manually mixed and then degassed under vacuum before being poured into either 4 inch square Petri dishes for the DIC, indentation, and RCC samples or 3 mL disposable plastic syringe barrels with torch sealed tips for the tension/torsion samples. The samples were subsequently cured at 70 °C for 21 hours after which they were removed and allowed to cool at room temperature for 5 days before any tests were performed. Cylinder samples were removed from the syringe barrel by first scoring the barrels with a Micro-Mark WonderCutter S and then pulling apart the barrel until it split in half. No visual indication of damage was observed on the cylinder surfaces. Samples for indentation were prepared by cutting out a square inch sample from the cured film. After indentation, RCC samples were prepared by punching out disks with a 5 mm diameter punch from this square inch film. A disk from this film was used to perform the compressional DMA described in the SI. Rectangular samples for uniaxial extension were cut from the same film source as the indentation sample.

1.2 Uniaxial extension

Uniaxial extension measurements were performed on a CellScale Biotester 5000 biaxial test machine equipped with a 23 N load cell. Rectangular samples of approximately 25 mm by 6 mm were loaded into the setup and clamped. Once clamped, the sample surface was sprinkled with 400 mesh graphite powder to create an optical speckle pattern. Samples were stretched at an extension rate of 1 mm s^{-1} (0.04 s^{-1}) to a

maximum extension of 10 mm. Deformation of the sample was visualized by a built-in CMOS tube camera at a resolution of 2048 by 2048 pixels and rate of 15 frames per second. DIC quantified the local deformations through the LabJoy software that comes with the instrument. A 9 by 16 grid of points was introduced on the sample frame before deformation was imposed and the positions of the points were tracked throughout the test. The initial dimensions of each cell were 0.676 mm by 0.416 mm or, given that there were 33.65 pixels per mm, 22.74 pixels by 14.00 pixels. A video showing the tracking of deformations during the test is shown in the SI. Additionally, E is extracted from these measurements in the SI and is found to be 2.27 ± 0.18 MPa.

1.3 Indentation and radially confined compression

Indentation was performed on a TA.XTPlus Connect Texture Analyzer equipped with a 50 N load cell. Indentation was performed with a 2 mm diameter flat steel cylinder. Square inch films with a thickness of ~2 mm were placed on a glass slide which was then put below the indenter. The initial indenter position was set to 3 mm above the top of the glass slide and a displacement rate of 0.1 mm s^{-1} (0.1 s^{-1}) was used to compress the film up to a turnaround force of 30 mN (max displacement measured as 11 ± 0.8 μm). The observed stiffness $\frac{F}{\delta}$ was used to calculate E from,[34]

$$E = \frac{3}{8R}\frac{F}{\delta}, \tag{3}$$

where R is the cylinder radius, F is force, and δ is displacement. The controlling software for the instrument corrected the reported displacement for the deflection of the instrument.

RCC was performed by compressing disks in a 5 mm diameter pellet die sourced from MSE Supplies and used as received. Samples were punched out with a 5 mm diameter punch (exact dimensions in SI) and loaded into the pellet die before the pellet die was loaded onto an Instron 5567 universal testing machine. The Instron was equipped with 100 kN capacity compression platens and a 30 kN force capacity load cell. Samples were tested by indenting at a rate of 1 μm s^{-1} (0.0005 s^{-1}) to a turnaround force of 4000 N, which translates to a max pressure of ~0.2 GPa. An instrument stiffness of 31.6 MN m^{-1} was measured in a run without a sample loaded into the die and this value was used to correct the observed displacement.

1.4 Tension and torsion of cylinders

An Admet eXpert 8602 axial-torsion testing machine equipped with a biaxial load cell with a 444.8 N force capacity and 11.3 N m torque capacity was used to perform tension and torsion on a single sample. This instrument is designed to translate in the axial direction and rotate to apply tension and/or torsion to a sample. The instrument is strain-controlled with the load and torque cell placed on the opposite side of the sample from the biaxial actuator. Fiducial markers were drawn on the surface of the 8.8 mm diameter cylinder samples before loading them into the drill chuck clamps. Samples had a height of ~30 mm with exact dimensions shown in the SI. Samples were subjected to axial extension at a rate of 1 mm s^{-1} (0.03 s^{-1}) up to a turnaround displacement of 5 mm before returning to the original position at a displacement of 0 mm. Once returned to the original position, the cylinder was twisted clockwise at a rate of 1° s^{-1} (0.0013 s^{-1} when radially averaged) to a turnaround angle of 45° before returning to the original position. Visualization of the test was provided by a Dino-Lite Edge Plus AM4117MZTW digital microscope (tube camera) with a resolution of 1280 by 960 pixels at 30 fps. An example video showing a typical testing protocol is shown in the SI.

2 ν Measured *via* digital image correlation

DIC is a measurement technique that uses the optical contrast provided by a speckle pattern to track local deformations during a test. DIC analysis was performed on rectangular strips that were extended uniaxially using the LabJoy software that comes integrated with the instrument. An example of this is shown in Fig. 2a where a grid of points is shown in the undeformed and deformed states. Here, the color of this grid indicates the strain value where blue is $\varepsilon_1 = 0$ and red is $\varepsilon_1 = 0.3$. These local deformations can be used to calculate the local

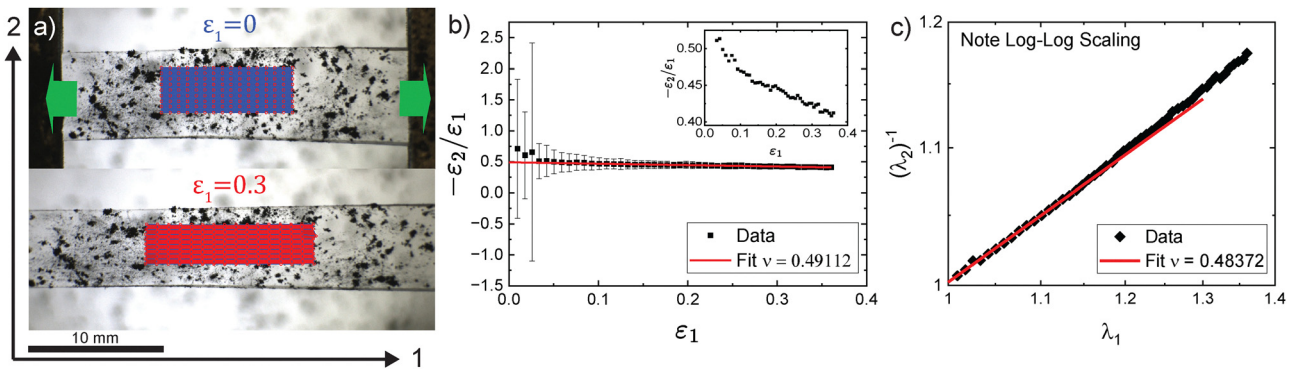

Fig. 2 (a) Images showing the stretching of rectangular strip with DIC overlay. (b) Plot of $-\frac{\varepsilon_2}{\varepsilon_1}$ *vs.* ε_1 used in the DIC ratio method. (c) Log–log plot of $(\lambda_2)^{-1}$ *vs.* λ_1 used in the DIC scaling method.

strains ε_i and stretches λ_i that are needed to estimate ν. Note that the stretches and strains are related as $\lambda_i = 1 + \varepsilon_i$.

ν can be estimated from the DIC data through one of two different methods. The first method takes advantage of the small strain definition of ν where,

$$\nu = -\frac{\varepsilon_2}{\varepsilon_1}, \tag{4}$$

when the 2 direction is the transverse direction and the 1 direction is the stretching direction during uniaxial extension. The calculation of ν from this direct ratio definition is shown in Fig. 2b where $-\frac{\varepsilon_2}{\varepsilon_1}$ is plotted against ε_1. This ratio was directly calculated and averaged across all grid points with the error bars being calculated as the standard deviation of this distribution as has been done by others.[9] Notably the error bars are large in the low strain regime where the displacements are similar in scale to the errors from DIC. The inset plot shows that, consistent with prior observations,[29] $-\frac{\varepsilon_2}{\varepsilon_1}$ decreases as ε_1 increases. This reduction results from a failure of the small strain definition of ν, not from an increase in the compressibility of the material. As shown in the SI, $-\frac{\varepsilon_2}{\varepsilon_1}$ should decrease at large strains for an incompressible material. Given the large errors that occur below $\varepsilon = 0.05$, the value of ν was calculated as the intercept from a linear extrapolation of the larger strain data. This fitting protocol from the direct ratio definition gives $\nu = 0.48 \pm 0.02$ when averaged across five samples.

A second method for measuring ν from DIC data uses a larger strain definition[30] where,

$$\nu = -\frac{\partial \ln(\lambda_2)}{\partial \ln(\lambda_1)} = \frac{\partial \ln\left((\lambda_2)^{-1}\right)}{\partial \ln(\lambda_1)}. \tag{5}$$

This definition of ν quantifies the scaling between λ_2 and λ_1 instead of a direct ratio of strains. Eqn (5) suggests that ν can be measured as the slope on a plot of $(\lambda_2)^{-1}$ *vs.* λ_1 when plotted on a logarithmic scale. An example of such a plot is shown in Fig. 2c where the slope is fit from $\lambda_1 = 1$ to $\lambda_1 = 1.15$. Repeating this analysis across five samples gives $\nu = 0.493 \pm 0.005$.

Notably, the direct ratio method results in an uncertainty value of $\Delta\nu = 0.02$ which is larger than the uncertainty value $\Delta\nu = 0.005$ observed with the scaling method. These uncertainty values set the number of significant figures with which ν should be reported. As is apparent from these values, the direct ratio method can quantify ν to two significant figures while the scaling method can report ν to three significant figures. This is consistent with the literature data in Fig. 1 which showed that reported DIC values of ν for nearly incompressible elastomers span a range of 2–3 significant figures. Ultimately, the difference in resolution between the two methods suggests that the scaling method is better at quantifying ν of nearly incompressible elastomers.

3 ν inferred from bulk and Young's modulus

An indirect approach for measuring ν is to infer its value from the measurement of two separate moduli. In this section, ν is inferred from measurements of E and K by rearranging eqn (2) to get,

$$\nu = \frac{1}{2} - \frac{E}{6K}. \tag{6}$$

Note that while E is used here in combination with K an analogous calculation could be performed by combining μ with K. The key part for inferring ν from these moduli is that they quantify different behavior for a material and therefore have different physical origins. E and μ characterize a material's resistance to changing shape and, in nearly incompressible elastomers, relate to the entropic penalty of stretching chains in a network.[35,36] On the other hand, K characterizes a material's resistance to changing volume and relates to the molecular interactions.[37,38] The different physical origin of these moduli is what makes them orders of magnitude apart.

Indentation was used to measure E as described in Section 1.3 and gave an estimate of $E = 2.27 \pm 0.08$ MPa. Note that E can be measured in different ways and indentation was selected here, instead of another method such as uniaxial extension, as

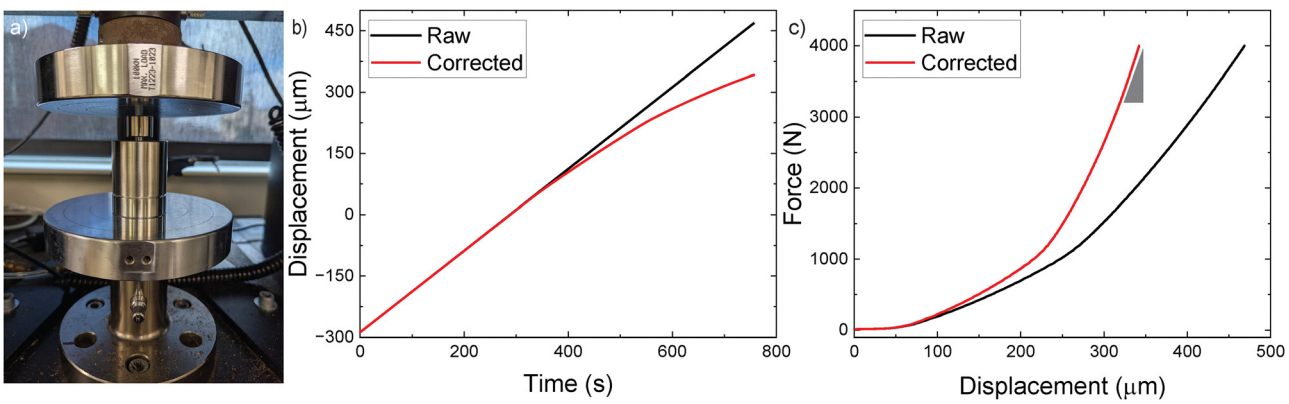

Fig. 3 (a) Image of the RCC setup. (b) Plot of displacement *vs.* time where displacement is zeroed to initial contact with the pellet die. (c) Plot of force *vs.* displacement for an example run where the slope on the corrected curve in the fully compacted regime is used to measure bulk modulus.

it is non-destructive and can be performed on the film used to punch out RCC disks. RCC was used to measure K and an image of the pellet die loaded into the compression setup is shown in Fig. 3a. A plot of the imposed displacement *vs.* time is shown in Fig. 3b. Note that the raw data reported by the Instron has been corrected for the deflection of the instrument by measuring the stiffness of the setup without a sample loaded into the pellet die. This stiffness was found to be 31.6 MN m^{-1} and the displacement was corrected by taking the raw displacement and subtracting the force divided by the instrument stiffness.

An example plot of force *vs.* displacement is shown in Fig. 3c for both the raw data and corrected data. Positive forces on this graph are compressive. Note that hydrostatic compression does not occur until full compaction of the material in the die. Once full compaction occurs K can be calculated as,[7,8]

$$\frac{\partial \sigma_z}{\partial \varepsilon_z} = \frac{3K(1-\nu)}{1+\nu} \approx K, \tag{7}$$

where σ_z and ε_z are the nominal stress and strain in the axial direction, respectively. The slope is taken near the maximum displacement to get the hydrostatic stiffness in the fully compacted regime. Note that this slope approaches K as $\nu \to 0.5$. As derived fully in the SI, the exact version of eqn (7) was used to calculate ν,

$$\frac{E}{\frac{\sigma_z}{\varepsilon_z}} = \frac{(1-2\nu)(1+\nu)}{(1-\nu)}, \tag{8}$$

where $\frac{\sigma_z}{\varepsilon_z}$ is the slope of the stress *vs.* strain curve. This measurement gave K = 4.2 ± 0.3 GPa averaged across five samples. When combined with E, the measurements of K give ν = 0.49991 ± 0.00001 averaged across five samples. This value shows that, consistent with the literature data in Fig. 1, RCC can provide an incredibly precise measurement of ν out to five significant figures.

The error associated with inferring ν from E and K can be understood by propagating the uncertainty from the moduli measurements. Derived fully in the SI, doing this yields,[39]

$$\Delta\nu = \frac{E}{6K}\sqrt{\left(\frac{\Delta E}{E}\right)^2 + \left(\frac{\Delta K}{K}\right)^2}. \tag{9}$$

Here it is apparent that any errors in measuring these two moduli are scaled by $\frac{E}{6K}$. Since E and K have different physical origins and are orders of magnitude apart, very precise measurements of ν can be inferred from this method. For example, eqn (9) predicts that the measurements in this work result in $\Delta\nu$ = 0.00002 which is in good agreement with the value calculated directly from the distribution of ν values. Based on this, it is clear that inferring ν from E and K provides a much more precise measurement than either of the DIC methods presented previously.

4 ν inferred from shear and Young's modulus

Another approach for measuring ν is to infer its value from measurements of E and μ. Performing such measurements have recently been proposed as a method to meaningfully quantify ν of nearly incompressible elastomers.[28,29] This

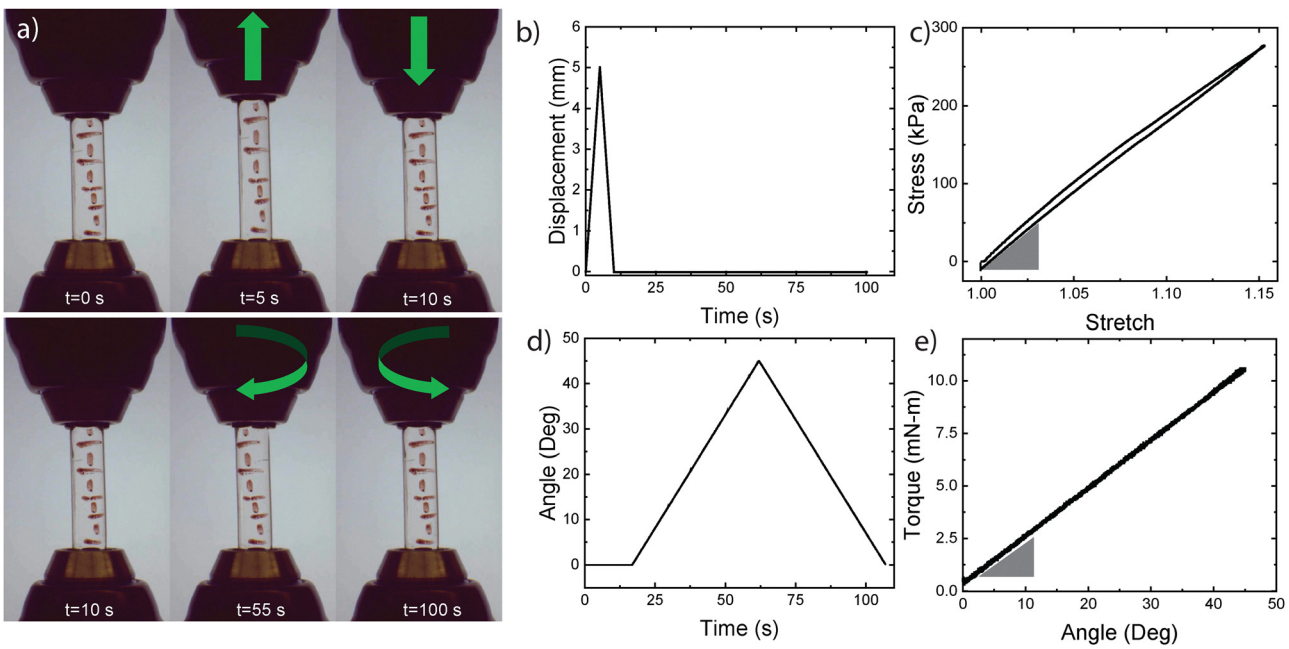

Fig. 4 (a) Images of the 8.8 mm diameter cylinder at different time points during the test. (b) Plot of the imposed displacement *vs.* time. (c) Plot of the measured stress *vs.* stretch where the slope in the low stretch regime gives E. (d) Plot of the imposed angle *vs.* time. (e) Plot of torque *vs.* angle that is used to measure the torsional stiffness.

proposed analysis derives from the fact that ν can be calculated from any two moduli,

$$\nu = \frac{E}{2\mu} - 1, \tag{10}$$

which is analogous to eqn (6) used in the previous section. A key difference here is that both E and μ characterize a material's resistance to changing shape and similarly derive from the entropic penalty of stretching chains in a rubbery polymer network. This means that these moduli are not separated by orders of magnitude as was the case when using K in the previous section.

In this work, inferring ν from E and μ is given its best chance of working by performing both moduli measurements on the same sample instead of combining measurements from different setups as was done in previous works.[28,29] Here that is accomplished by using a combined tension and torsion tester to first stretch the samples and then twist the samples. Note that the uniaxial extension measurements used here to characterize E are distinct from the indentation measurements used in the previous section. Images of this testing protocol can be seen in Fig. 4a. Plots showing displacement *vs.* time and angle *vs.* time are shown in Fig. 4b and d, respectively. These plots show that first the sample is subjected to uniaxial extension before unloading. E is measured as the low strain slope on the loading curve as can be seen on a plot of stress *vs.* stretch in Fig. 4d. These measurements give $E = 2.47 \pm 0.14$ MPa across five samples. This E value shows reasonable agreement with the value of $E = 2.27 \pm 0.08$ MPa measured *via* indentation.

After the tension is removed from the sample it is twisted to apply torsion. μ is measured as,[40]

$$\mu = \frac{M_z}{\theta}\frac{2L}{\pi R^4}, \tag{11}$$

where M_z is the moment about the z axis, θ is the applied angle of rotation, L is the length of the cylinder, and R is the radius of the cylinder. The torsional stiffness $\frac{M_z}{\theta}$ is measured from a plot of torque *vs.* angle as shown in Fig. 4e and gives $\mu = 0.79 \pm 0.07$ MPa measured across five samples.

Note that the values of ν were not calculated from the averaged moduli values. Instead each sample's measurement of E and μ was used to directly calculate an estimate of ν as can only be done when both measurements are performed on the same sample. Doing this, gives $\nu = 0.56 \pm 0.09$ when ν is then averaged across five samples. The observation that $\Delta\nu = 0.09$ is consistent with the literature reported values shown in Fig. 1.

Table 1 contains a summary of the observed values of ν for all of the methods presented in this work. This data is plotted in the SI. This data suggests that inferring ν from μ and E is the worst possible method while inferring it from K and E is the best possible method. This difference in precision between the two methods can be understood by propagating the error,[39] as shown fully in the SI, from the moduli measurements to get,

$$\Delta\nu = \frac{E}{2\mu}\sqrt{\left(\frac{\Delta E}{E}\right)^2 + \left(\frac{\Delta\mu}{\mu}\right)^2}. \tag{12}$$

This shows that the propagated error from the measurement of these moduli is scaled by $\frac{E}{2\mu}$. Given that $\frac{E}{\mu} = 3$ when $\nu = 0.5$, the error that propagates from the measurement of μ and E will increase by a factor of 1.5 through this method. This in stark contrast to the previous section where the propagated error was reduced by orders of magnitude. This implies that reasonable measurements of μ and E can result in large errors for ν. For example, plugging the values in this section into eqn (12) gives $\Delta\nu = 0.16$. While there appears to be less error when $\Delta\nu$ is directly calculated from a distribution of ν this is only possible when performing measurements on a single sample as is done in this work. Regardless, the fact that this method only gives one decimal point of resolution means that the value of Poisson's ratio for nearly incompressible elastomers cannot be meaningfully inferred from measurements of μ and E.

Table 1 Values of ν calculated from the four methods reported in this work. Each reported value represents a measurement on five samples

Method	ν
DIC (ratio)	0.48 ± 0.02
DIC (scaling)	0.493 ± 0.005
Inferred from K and E	0.49991 ± 0.00001
Inferred from μ and E	0.56 ± 0.09

5 Impact of cumulative errors

Discussion in the previous sections largely focused on the precision with which ν can be estimated *via* different methods. This section is focused on the accuracy of each method of estimating ν. The importance of this discussion can be seen in Table 1 where the observed $\Delta\nu$ values are all reasonably consistent with the error propagation arguments presented previously. However, such arguments fail to explain why the mean values for each method do not appear to be the same value reported out to different significant figures. For example, a researcher using the direct ratio DIC method may, upon observing that $\nu = 0.48$, reasonably decide that much of the discussion in the previous sections does not apply to their system as a measured value of $\nu = 0.48$ suggests the material is well into the compressible regime. Were $\nu = 0.48$ an accurate value it could be combined with a value of $E = 2.47$ MPa in eqn (2) to predict that $K = 20.6$ MPa whereas RCC measurements show that $K = 4.2$ GPa for this material. With these observations in mind, it is important to question how sensitive the mean reported value of ν is to experimental errors.

The first step towards addressing this question comes in remarking on the fact that every experimental measurement is associated with some amount of error. This variability results in a distribution of values that are measured. While replicates are typically run in lab, measurements only sample a subset of this distribution of values. The hope is that the reported mean and standard deviation of this sampling is representative of the "true" value of the measured property. This means that the sensitivity of a measured value of ν to experimental errors can be quantified by assuming a "true" value of ν. For example, assuming the "true" value of ν is the incompressible value of

0.5 gives,

$$\nu_{\text{ratio}} = -\frac{\varepsilon_2}{\varepsilon_1} = 0.5\left(\frac{100 + C}{100}\right), \tag{13}$$

for the ratio DIC method where C is the cumulative error of the measurement in %. In other words, the $\frac{100 + C}{100}$ term quantifies how far the observed value of ν is from the "true" value of 0.5 for a given error level. C represents the cumulative error that results from combining the individual errors of the measured values of ε_1 and ε_2. A similar analysis can be performed for the scaling DIC method and gives,

$$\nu_{\text{scaling}} = -\frac{\partial \ln(\lambda_2)}{\partial \ln(\lambda_1)} = 0.5\left(\frac{100}{100 + C}\right). \tag{14}$$

Both equations are plotted in Fig. 5 and show that small measurement errors can result in significant differences in the mean value of ν. For example, to see $\nu = 0.48$ from the DIC ratio method only requires $C \approx -4\%$. Similarly, the value of $\nu = 0.493$ observed in the DIC scaling method would only require $C \approx 1.5\%$. This shows that cumulative errors below 5% can have significant impact on the observed value of ν. Further it can be seen in Fig. 5, that it only takes a cumulative error of about 10% to report values of $\nu = 0.45$. Seeing as DIC methods are essentially equivalent to the strain gauge methods commonly used in the classical literature, this analysis has wide-ranging implications for the reported values of ν for materials that should be nearly incompressible, yet are observed to be in the compressible regime.[28–30,41,42]

This analysis can be further extended to the indirect calculation methods. If a true value of $\nu = 0.5$ is assumed then $\frac{E}{\mu} = 3$ which gives,

$$\nu_{\text{apparent}} = \frac{E}{2\mu} - 1 = \frac{3}{2}\left(\frac{100 + C}{100}\right) - 1. \tag{15}$$

A cumulative error analysis that assumes a "true" value of $\nu = 0.5$ is incompatible with eqn (6). Instead a cumulative error analysis is performed by assuming that $E = 1$ MPa and $K = 1$ GPa are "true" values for the moduli which gives,

$$\nu_{\text{apparent}} = \frac{1}{2} - \frac{E}{6K} = \frac{1}{2} - \frac{1}{6000}\left(\frac{100 + C}{100}\right). \tag{16}$$

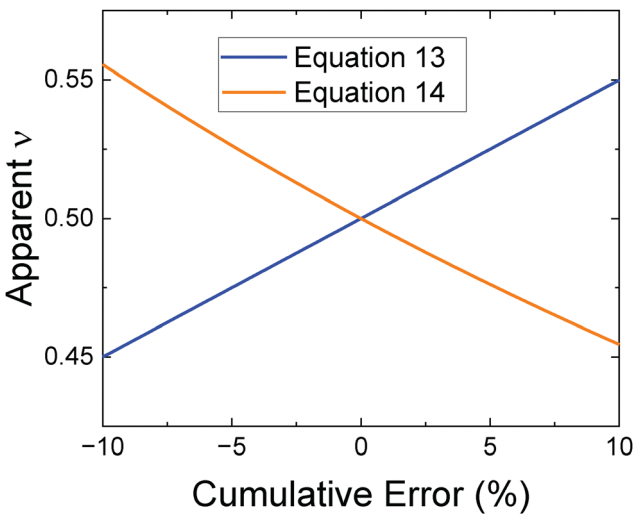

Fig. 5 Plot showing how cumulative error can shift the apparent value of ν when using DIC methods.

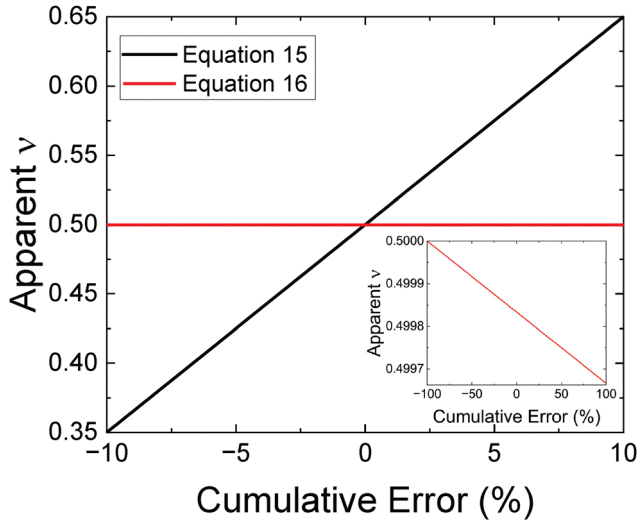

Fig. 6 Plot showing how cumulative error can shift the apparent value of ν when inferring it from moduli measurements.

Both of these equations are plotted in Fig. 6. This plot shows that the observed value of $\nu = 0.56$ for inferring from μ and E would only require $C \approx 4\%$. Further, it can be seen on this plot that this method is the most susceptible method to cumulative error. Notably, it only takes a cumulative error of 10% to see an apparent value of $\nu = 0.35$ which likely explains some of the more extreme values reported in the literature.[28] On the other hand, a cumulative error of 100% only decreases the apparent value of ν to 0.49965 when inferring it from measurements of K and E. This demonstrates that inferring ν from measurements of K and E is a superior method for nearly incompressible materials that demand both high accuracy and high precision. All other methods presented in this work lack the precision and accuracy to meaningfully distinguish values of ν in the nearly incompressible regime ($\nu > 0.495$) from the incompressible limit of $\nu = 0.5$. Further, future researchers attempting to measure ν for nearly incompressible materials need to carefully consider the impact that cumulative errors have on their measurement of Poisson's ratio.

6 Conclusions

An experimental comparison of three methods of characterizing Poisson's ratio of nearly incompressible elastomers was performed. Arguments quantifying how experimental errors impact both the precision and accuracy of the measurement were presented. Of the methods tested, inferring ν from a measurement of the bulk modulus and Young's modulus was found to perform the best. This performance resulted from the

different physical origins of each modulus making them orders of magnitude apart. This difference ends up scaling down any experimental errors. Further it was found that DIC and inferring ν from measurements of the shear and Young's modulus lacked the resolution to meaningfully distinguish values of ν from the incompressible limit of 0.5. Notably, the discussion of the impact of cumulative errors has practical implications for future measurements of $\nu > 0.495$ in the nearly incompressible regime. These findings are relevant to understanding the mechanical response of rubbery materials under hydrostatic loadings.

Conflicts of interest

The authors declare no conflicts of interest.

Data availability

The data supporting this article have been included as part of the SI.

SI videos, compiled literature data, derivations of equations, and further experimental details. See DOI: **https://doi.org/10.1039/d5sm00535c**

Acknowledgements

This work was supported by the National Science Foundation ReDDDoT program through grant 2427693.

References

1 C. Creton and M. Ciccotti, *Rep. Prog. Phys.*, 2016, **79**, 046601.
2 G. A. Tizard, D. A. Dillard, A. W. Norris and N. Shephard, *Exp. Mech.*, 2012, **52**, 1397–1405.
3 Y.-H. Lai, D. A. Dillard and J. S. Thornton, *J. Appl. Math. Mech.*, 1992, **60**, 787.
4 R. Hensel, R. M. McMeeking and A. Kossa, *J. Adhes.*, 2019, **95**, 44–63.
5 C. Logeais, C. Ovalle and L. Laiarinandrasana, *Mech. Mater.*, 2025, **200**, 105193.
6 R. S. Rivlin and D. W. Saunders, *Philos. Trans. R. Soc., A*, 1951, **243**, 251–288.
7 B. P. Holownia, *Rubber Chem. Technol.*, 1975, **48**, 246–253.
8 C. W. Barney, M. E. Helgeson and M. T. Valentine, *Extreme Mech. Lett.*, 2022, **52**, 101616.
9 R. H. Pritchard, P. Lava, D. Debruyne and E. M. Terentjev, *Soft Matter*, 2013, **9**, 6037–6045.
10 Y.-X. Xu and J.-Y. Juang, *Polymers*, 2021, **13**, 1498.
11 L. I. Farfan-Cabrera, J. B. Pascual-Francisco, O. Barragan-Perez, E. A. Gallardo-Hernandez and O. Susarrey-Huerta, *Polym. Test.*, 2017, **59**, 245–252.
12 S. Dogru, B. Aksoy, H. Bayraktar and B. E. Alaca, *Polym. Test.*, 2018, **69**, 375–384.
13 L. I. Farfan-Cabrera and J. B. Pascual-Francisco, *Exp. Mech.*, 2022, **62**, 287–297.
14 T. L. Smith, *J. Polym. Sci.*, 1958, **32**, 99–113.
15 J. C. Smith, G. A. Kermish and C. A. Fenstermaker, *J. Adhes.*, 1972, **4**, 109–122.
16 A. Müller, M. C. Wapler and U. Wallrabe, *Soft Matter*, 2019, **15**, 779–784.
17 Z. Laufer, Y. Diamant, M. Gill and G. Fortuna, *Int. J. Polym. Mater.*, 1978, **6**, 159–174.
18 U. Yilmazer and R. J. Farris, *J. Appl. Polym. Sci.*, 1983, **28**, 3369–3386.
19 C. Weir, *J. Res. Natl. Bur. Stand.*, 1953, **50**, 153.
20 L. H. Adams and R. E. Gibson, *J. Wash. Acad. Sci.*, 1930, **20**, 213–223.
21 L. A. Wood and G. M. Martin, *Rubber Chem. Technol.*, 1964, **37**, 850–865.
22 A. H. Scott, *J. Res. Natl. Bur. Stand.*, 1935, **14**, 99–120.
23 G. K. Rightmire, *J. Lubr. Technol.*, 1970, **92**, 381–386.
24 K. L. Fishman and D. Machmer, *J. Test. Eval.*, 1994, **22**, 161–167.
25 M. Stanojevic and G. K. Lewis, *Polym. Test.*, 1983, **3**, 183–195.
26 B. P. Holownia, *J. Strain Anal. Eng. Des.*, 1972, **7**, 236–242.
27 D. T. Clelland, E. K. Nickerson and D. R. Merkel, *Polym. Test.*, 2023, **125**, 108135.
28 A. M. Smith, D. G. Inocencio, B. M. Pardi, A. Gopinath and R. C. A. Eguiluz, *ACS Appl. Polym. Mater.*, 2024, **6**, 2405–2416.
29 S. Pal and A. Bhattacharyya, *Polym. Test.*, 2025, **143**, 108687.
30 T. L. Smith, *Trans. Soc. Rheol.*, 1959, **3**, 113–136.
31 P. B. Lindley, *J. Strain Anal.*, 1979, **14**, 11–16.
32 K. Efimenko, W. E. Wallace and J. Genzer, *J. Colloid Interface Sci.*, 2002, **254**, 306–315.
33 D. Ortiz-Acosta and C. Densmore, *Sylgard Cure Inhibition Characterization*, Los alamos national laboratory technical report, 2012.
34 I. N. Sneddon, *Int. J. Eng. Sci.*, 1965, **3**, 47–57.
35 P. J. Flory, *Chem. Rev.*, 1944, **35**, 51–75.
36 C. W. Barney, Z. Ye, I. Sacligil, K. R. Mcleod, H. Zhang, G. N. Tew, R. A. Riggleman and A. J. Crosby, *Proc. Natl. Acad. Sci. U. S. A.*, 2022, **119**, 1–6.
37 D. Tabor, *Polymer*, 1994, **35**, 2759–2763.
38 N. B. Shenogina, M. Tsige, S. S. Patnaik and S. M. Mukhopadhyay, *Macromolecules*, 2012, **45** 5307–5315.
39 H. H. Ku, *J. Res. Natl. Bur. Stand., Sect. C*, 1966, **70C**, 263–273.
40 A. S. Saada, *Elasticity Theory and Applications*, J. Ross Publishing, Inc., 2nd edn, 2009.
41 K. Urayama, T. Takigawa and T. Masuda, *Macromolecules*, 1993, **26**, 3092–3096.
42 T. Takigawa, Y. Morino, K. Urayama and T. Masudab, *Polym. Gels Networks*, 1996, **4**, 1–5.

